Ceramics International 43 (2017) 6013–6018

Contents lists available at ScienceDirect

Ceramics International

journal homepage: www.elsevier.com/locate/ceramint

Role of nitrogen-related complex in stabilizing ferromagnetic ordering in a rare-earth and nitrogen codoped ZnO

Jinhuan Jia[a], Yongfeng Li[a,b,*], Bin Yao[a,b], Zhanhui Ding[a], Ruijian Liu[a], Rui Deng[c], Ligong Zhang[d], Haifeng Zhao[d], Lei Liu[d]

[a] State Key Lab of Superhard Material and College of Physics, Jilin University, Changchun 130012, China
[b] Key Laboratory of Physics and Technology for Advanced Batteries (Ministry of Education), College of Physics, Jilin University, Changchun 130012, China
[c] School of Materials Science and Engineering, Changchun University of Science and Technology, Changchun 130022, China
[d] State Key Lab of Excited State Processes, Changchun Institute of Optics, Fine Mechanics and Physics, Chinese Academy of Sciences, Changchun 130033, China

ARTICLE INFO

Keywords:
ZnO
Diluted magnetic semiconductor
Ferromagnetism
Magnetron sputtering
First-principle calculation

ABSTRACT

We report the ferromagnetic enhancement in a rare-earth and nitrogen co-doped ZnO thin film. To reveal the origin of ferromagnetism, we perform a comparative study on undoped, Nd-doped, N-doped and (Nd, N)-codoped ZnO thin films by combining experiments with first-principles calculations. Compared with the Nd-doped ZnO, the N incorporation into the Nd-doped ZnO to form $2Nd_{Zn}$-N_O complex leads to the more stable ferromagnetic coupling between two Nd atoms, which is well supported by first-principles calculations. Our results suggest that the electronic structure alteration via codoping engineering plays a critical role in stabilizing the ferromagnetic orderings.

1. Introduction

Over the past two decades, diluted magnetic semiconductors (DMSs) have attracted much attention due to their potential applications in spin electronics and magnetic devices [1,2]. Compared with the conventional semiconductor, cations in DMSs are partly substituted by magnetic ions so that DMSs are expected to have high Curie temperature (T_C) exceeding room temperature [3,4] and utilize both charge and spin degrees of freedom [1,5–7]. The novel behavior of DMSs leads to the potential applications in the new emerging fields of semiconductor spintronic devices, spin polarized light emitting diodes, photovoltaics and sensors [8–13]. Among the various material candidates as DMSs [14,15], most of researches have been mainly focused on ZnO owing to the theoretically predicted room temperature ferromagnetism [16–20]. Furthermore, ZnO has excellent properties, such as a direct wide-bandgap of 3.37 eV and a large exciton binding energy of 60 meV at room temperature [21–23]. Although room temperature ferromagnetism in transition metals (TMs) doped ZnO has been reported, the magnetism is often weak [24]. Compared with TMs, rare-earth (RE) metals with open f shells, often offer larger magnetic moment. Indeed, both theoretical and experiments studies revealed that Gd-doped GaN exhibits a colossal magnetic moment [25,26]. Therefore, it remains an open question whether RE doping can induce strong room temperature ferromagnetism in ZnO. However, up to now, RE elements have been much less pursued as dopants in ZnO that shows room temperature ferromagnetism, even if recent theoretical and experiments studies have indicated that RE-doped (RE=Gd, Nd) doped ZnO films only show paramagnetic behavior or very weak ferromagnetism at room temperature [27–30]. In the recent years, the codoping approach, especially donor-acceptor cooping, has been intensively studied due to the possibility to tailor the position and occupancy of the Fermi energy of doped DMSs [31]. For instance, Wang *et al.* observed room temperature ferromagnetism in the (Mn, N)-codoped ZnO [32]. In our previous work, it was also observed that donor-acceptor complex in SnO_2 induce room temperature ferromagnetism [33]. Therefore, codoping is likely to be a potential approach to enhance the ferromagnetism of ZnO.

In this article, we conducted a comparative study on undoped, Nd-doped, N-doped and (Nd, N)-codoped ZnO via complementary experiments and first-principles calculations based on spin-polarized density functional theory (DFT). In the (Nd, N)-codoped ZnO thin film, we observed ferromagnetic enhancement at room temperature. The first-principles calculations reveal that the N incorporation into the Nd-doped ZnO results in the more stable ferromagnetic ordering between two Nd atoms, which well supports our experimental results.

* Corresponding author at: State Key Lab of Superhard Material and College of Physics, Jilin University, Changchun 130012, China.
E-mail addresses: liyongfeng@jlu.edu.cn (Y. Li), binyao@jlu.edu.cn (B. Yao).

http://dx.doi.org/10.1016/j.ceramint.2017.01.140
Received 12 December 2016; Received in revised form 26 January 2017; Accepted 28 January 2017
Available online 31 January 2017

2. Experimental and first-principles calculations details

Undoped, Nd-doped, N-doped and (Nd, N)-copded ZnO films were deposited on c-plane sapphire substrates by radio-frequency (RF) magnetron sputtering. The pure and Nd-doped ZnO ceramic targets were sintered by high purity ZnO (99.99%, Alfa Aesar) and the mixture of the ZnO and Nd_2O_3 (99.99%, Alfa Aesar) powder with a mole ratio of 99:1, respectively. The pressure of the growth chamber was evacuated to be 3×10^{-4} Pa before deposition, and then filled with sputtering gas and was kept at 1.0 Pa during depositing process. The pure Ar gas was used as work gas for the undoped and Nd-doped ZnO films, and the mixed gases of Ar and N with a flow ratio of 3:1 for the N-doped and (Nd, N)-codoped ZnO films. All thin films were sputtered for 1 h at deposition temperature of 500 °C.

X-ray diffraction (XRD) was used to determine crystal structures using an X-ray diffractometer with Cu *Kα* radiation (λ=0.15418 nm). Chemical states and compositions were determined using X-ray photoelectron spectroscopy (XPS). The adventitious C 1*s* peak at 284.6 eV was used to calibrate the binding energy. The concentrations of Nd and N for the Nd-doped and N-doped ZnO films were determined to be 2.8 at% and 1.0 at%, as well as 2.6 at% and 1.8 at% for the (Nd, N)-codoped ZnO films, respectively. Magnetization measurements were performed using a superconducting quantum interference device magnetometer (SQUID, Quantum Design, MPMSXL-5). The optical absorption measurements were performed using a UV–vis–near-IR spectrophotometer. The photoluminescence (PL) measurements were performed using a He–Cd laser with a 325-nm line as the excitation source.

In the first-principles calculations based on density functional theory (DFT), we adopted the VASP code with the projector augmented wave (PAW) potentials for the electronic interaction and the generalized gradient approximation (GGA) for the electron exchange and correlation [34–37]. The cutoff energy of 400 eV for the plane-wave basis was used and a 72-atom 3×3×2 supercell with the wurtzite structure was constructed. In the ZnO supercells, we constructed three different configurations for simulating the doped ZnO: (i) Two nearest-neighbor O atoms are substituted by two N atoms to form N_O-N_O configuration; (ii) Two nearest-neighbor Zn atoms are substituted by two Nd atoms to form Nd_{Zn}-Nd_{Zn} configuration; (iii) One O atom between two Nd atoms are substituted by one N atom to form $2Nd_{Zn}$-N_O complex. For the Brillouin-zone integration, a 3×3×3 Monkhorst-Pack k-point mesh was used; a more refined (8×8×8) k-point mesh was used for the density-of-states (DOS) calculations. In the supercell optimization calculations, all the atoms are allowed to relax until the Hellmann-Feynman forces acting on them become less than 0.01 eV/Å.

3. Results and discussion

Fig. 1 shows the XRD patterns of undoped ZnO, Nd-doped ZnO, N-doped ZnO and (Nd, N)-codoped ZnO films grown on *c*-Al_2O_3 substrates. For all the samples, only ZnO (002) diffraction peak is observed, indicating the ZnO films have the wurtzite structure with a preferred orientation and no impurity phase is detected. The enlarged ZnO (002) peaks are shown in the right panel of Fig. 1 for clearly demonstrating the peak positions. The (002) diffraction peaks of the doped ZnO films have a shift towards low diffraction angle with respect to the undoped ZnO films. The ionic radii of the Nd, Zn, N and O are 0.98, 0.74, 1.46 and 1.40 Å determined by Shannon [38]. The larger ionic radius of Nd and N than Zn and O lead to the lattice expansion, resulting in the peak shift towards to low diffraction angle. Therefore, the diffraction peak shifts confirm that the corresponding doping atoms are incorporated into ZnO lattices.

To determine the chemical states of dopants in ZnO, XPS measurements were carried out. Fig. 2(a) shows the XPS spectra of Nd 3*d* in the ZnO:Nd and ZnO:(Nd,N) films. The binding energy values obtained for Nd $3d_{3/2}$ and Nd $3d_{5/2}$ are 998.7 and 982.1 eV, respectively, confirming the trivalent state of Nd in the Nd doped and (Nd, N)-codoped ZnO films [39]. Fig. 2(b) shows the XPS spectra of N 1*s* in the ZnO:N and ZnO:(Nd,N) films. The N 1*s* spectrum displays one peak at 395.8 eV. It should be pointed that the binding energy of N 1*s* state varies from 395 to 408 eV as chemical environment of nitrogen atom changes [40]. The peak at 396 eV is assigned to nitrogen substitution at oxygen site (N_O), acting as acceptor [41].

Fig. 3 shows the optical absorption data of $(\alpha h\nu)^2$ versus $h\nu$, where α is the absorption coefficient and $h\nu$ is the photon energy. Using Tauc rule [42]: $\alpha h\nu \propto (h\nu - E_g)^{1/2}$, the bandgaps of undoped ZnO, N-doped ZnO, Nd-doped ZnO and (Nd, N)-codoped ZnO are 3.29, 3.26, 3.33 and 3.31 eV, respectively. The bandgap of the N-doped ZnO is slightly smaller than the undoped ZnO, which is ascribed to the occurrence of band tail states introduced by N acceptor incorporation. The bandgap of the Nd-doped and (Nd, N)-codoped ZnO is significantly larger than the undoped ZnO, which is due to Burstein-Moss effect [43,44]. It should be noted that the absorption edge of the (Nd, N)-codoped ZnO is smaller than the Nd-doped ZnO. The doped Nd and N atoms act as donors and acceptors in ZnO film, respectively. As a result, a passivated donor-acceptor impurity band can occur in the bandgap when a large

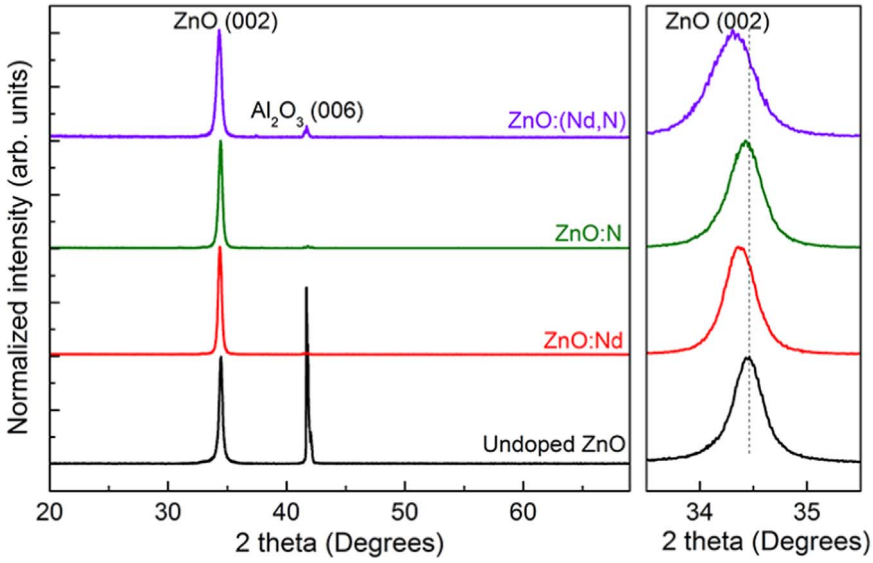

Fig. 1. Normalized XRD patterns of the undoped, Nd-doped, N-doped and Nd-N codoped ZnO thin films. The enlarged ZnO (002) peaks are shown in the right panel.

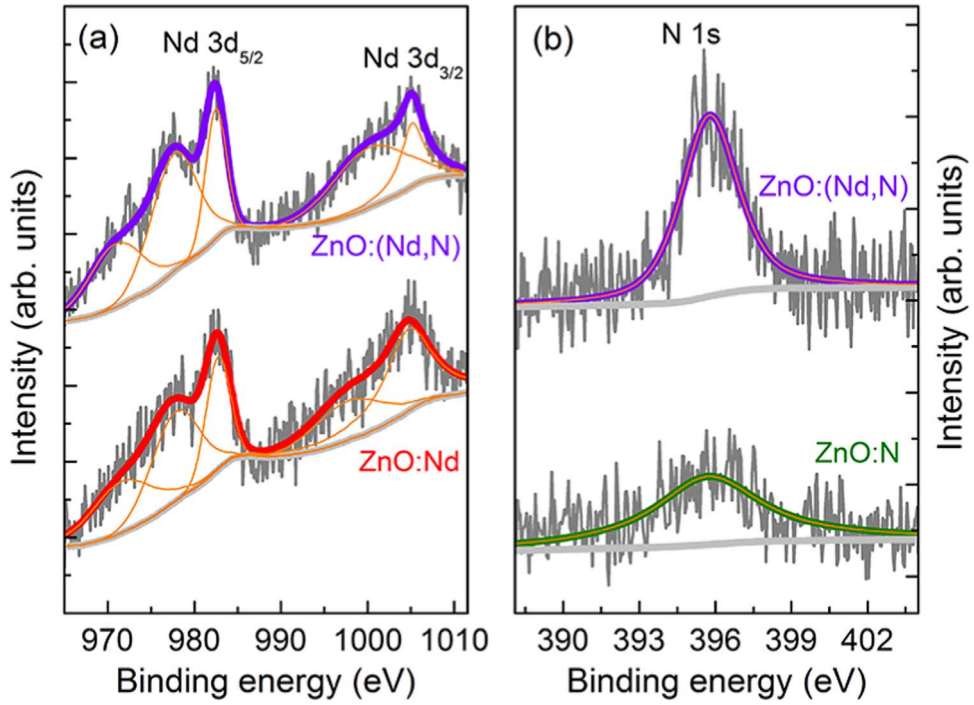

Fig. 2. XPS spectra of (a) Nd 3d states in the ZnO:Nd and ZnO:(Nd,N) thin films as well as (b) N 1s states in the ZnO:N and ZnO:(Nd,N) thin films.

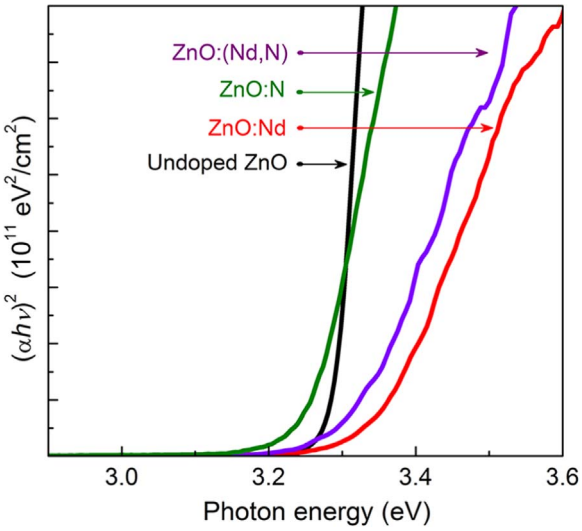

Fig. 3. The $(ahv)^2$ versus hv of the undoped ZnO, ZnO:Nd, ZnO:N and ZnO:(Nd,N) thin films.

number of donor-acceptor complexes are presented in the film [45]. Therefore, the narrowing of band gap is attributed to the emergence of the donor-acceptor complexes.

Fig. 4(a) shows the raw data of magnetization versus magnetic field (M-H) measured at room temperature for the undoped, Nd-doped, N-doped and (Nd, N)-codoped ZnO thin films, without subtracting the substrate contribution. The M-H curve of the ZnO:(Nd,N) clearly exhibits ferromagnetic behavior superimposed on diamagnetism from sapphire substrates. Fig. 4(b) shows the M-H curves after subtracting the diamagnetic contributions from the sapphire substrates. For the undoped and Nd-doped ZnO films, the M-H curves include paramagnetic and weak ferromagnetic behavior. The weak ferromagnetism is attributed to intrinsic defects in ZnO [16,46–49]. The observed paramagnetic behavior in the Nd-doped ZnO is consistent with the previous reports [27]. The ferromagnetic behavior is observed for the N-doped and (Nd, N)-codoped ZnO films. Compared with the N-doped

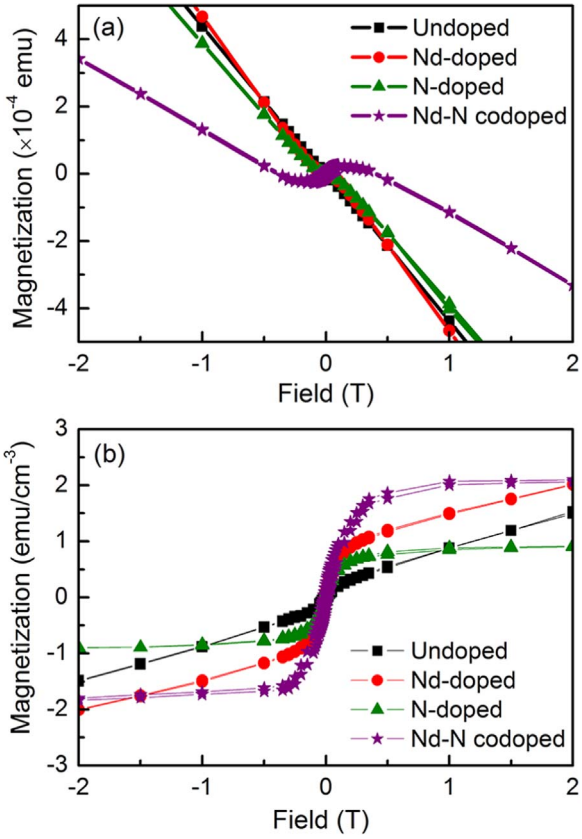

Fig. 4. (a) Magnetization versus magnetic field curve at room temperature for the undoped ZnO, ZnO:Nd, ZnO:N and ZnO:(Nd,N) thin films. (b) The corresponding ferromagnetic hysteresis loops after subtracting the diamagnetic contribution from the substrates.

ZnO, the (Nd, N)-codoped ZnO shows a double ferromagnetic enhancement, indicating the (Nd, N)-codoping plays an important role in enhancing ferromagnetism of ZnO.

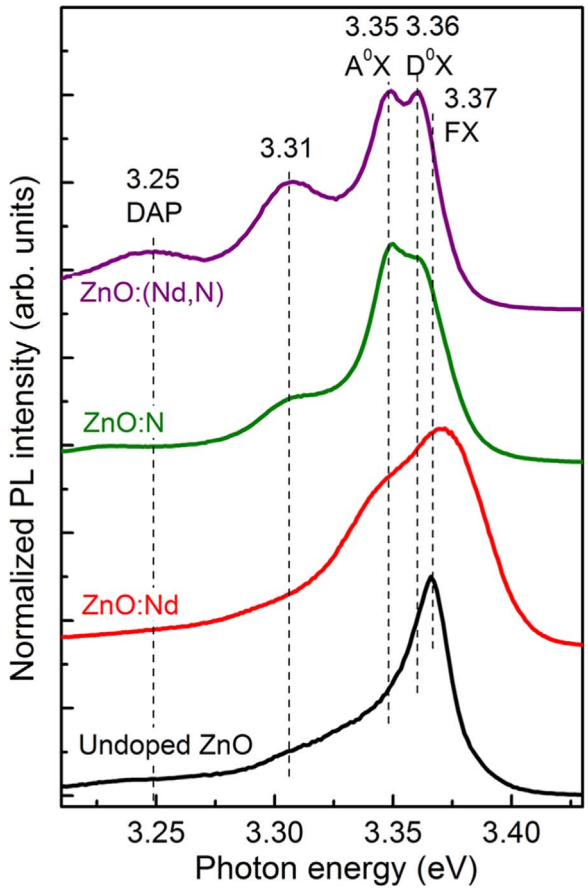

Fig. 5. 80 K PL spectra of the undoped ZnO, ZnO:Nd, ZnO:N and ZnO:(Nd,N) thin films.

To search for the possible defects related to the origin of ferromagnetism, we performed low temperature PL measurement because PL is an effective tool to reveal the defect characteristics in semiconductors. Fig. 5 shows the 80 K PL spectra of undoped ZnO, Nd-doped ZnO, N-doped ZnO and (Nd, N)-codoped ZnO films. For the undoped ZnO film, a sharp peak is found at 3.37 eV, which is assigned to radiative recombination of free exciton (FX) [50,51]. The observation of FX indicates that the prepared sample is of high quality. The emission peak of the Nd-doped ZnO film shows a blueshift with respect to the undoped ZnO, which is attributed to Burstein–Moss effect [43,44]. The N-doped ZnO film exhibits three near-band-edge (NBE) peaks at 3.36 eV, 3.35 eV and 3.31 eV. The emission at 3.36 eV can be unambiguously assigned to excitons bound to the neutral donors (D^0X) [43,44], which is due to the donor defects of ZnO. The emission around 3.35 eV is ascribed to the excitons bound to the neutral acceptors (A^0X), which is related to N acceptor doping. The origin of 3.31 eV PL emission is due to the stacking faults related to acceptors [52,53]. For the (Nd, N)-codoped ZnO films, besides the peaks at 3.36 eV, 3.35 eV and 3.31 eV, an obvious emission peak at 3.25 eV is observed, which originates from radiative recombination of donor-acceptor pairs (DAP) [54]. The emergence of the DAP emission is likely to related to the of the ferromagnetic property of (Nd, N)-codoped ZnO as we will discuss later.

The electrical properties of the undoped, Nd-doped, N-doped and (Nd, N) codoped films are summarized in Table 1. The undoped ZnO film show an n-type conduction with an electron concentration of 5.3×10^{18} cm^{-3} and high mobility of 14.7 $cm^2\ V^{-1}\ s^{-1}$. The electron concentration of the Nd-doped ZnO film increases to 3.5×10^{20} cm^{-3} due to the incorporation of shallow Nd donor. A p-type conduction with a hole concentration of ~10^{17} cm^{-3} is obtained for the N-doped ZnO film. The p-type conduction is due to N substituting O site as an acceptor in ZnO. Interestingly, a significant decrease of carrier concentration is observed for the (Nd, N)-codoped ZnO due to the compensation of N acceptors to Nd donors.

Table 1
The electrical properties of the undoped and doped ZnO thin films.

Doping element	Resistivity (Ω cm)	Carrier density (cm^{-3})	Mobility ($cm^2\ V^{-1}\ s^{-1}$)	Conduction type
undoped	0.08	5.3×10^{18}	14.7	n
Nd	1.5×10^{-3}	3.5×10^{20}	11.9	n
N	85.5	2.4×10^{17}	0.3	p
Nd-N	0.02	1.2×10^{20}	2.6	n

To check the stability of ferromagnetic couplings, the electronic structures and total energies of Nd-doped, N-doped and (Nd, N)-codoped ZnO systems were calculated using first-principles methods. We constructed the three different ZnO supercell configurations: N_O-N_O, Nd_{Zn}-Nd_{Zn} configurations and $2Nd_{Zn}$-N_O complex. The energy differences between antiferromagnetic (AFM) and ferromagnetic (FM) states ($\Delta E=E_{AFM}-E_{FM}$) for the N_O-N_O, Nd_{Zn}-Nd_{Zn} configurations and $2Nd_{Zn}$-N_O complex are 40, 18 and 104 meV, respectively. The small ΔE value for the Nd_{Zn}-Nd_{Zn} configuration indicates a paramagnetic behavior, which is in agreement with the previous reports [27]. The ΔE value for the N_O-N_O configuration is consistent with the calculated result of 44 meV by Wang et al. [55] and is also in accordance with the weak ferromagnetism of ZnO:N observed experimentally [56]. In these configurations, the large ΔE for the $2Nd_{Zn}$-N_O complex indicates the most stable FM coupling, well

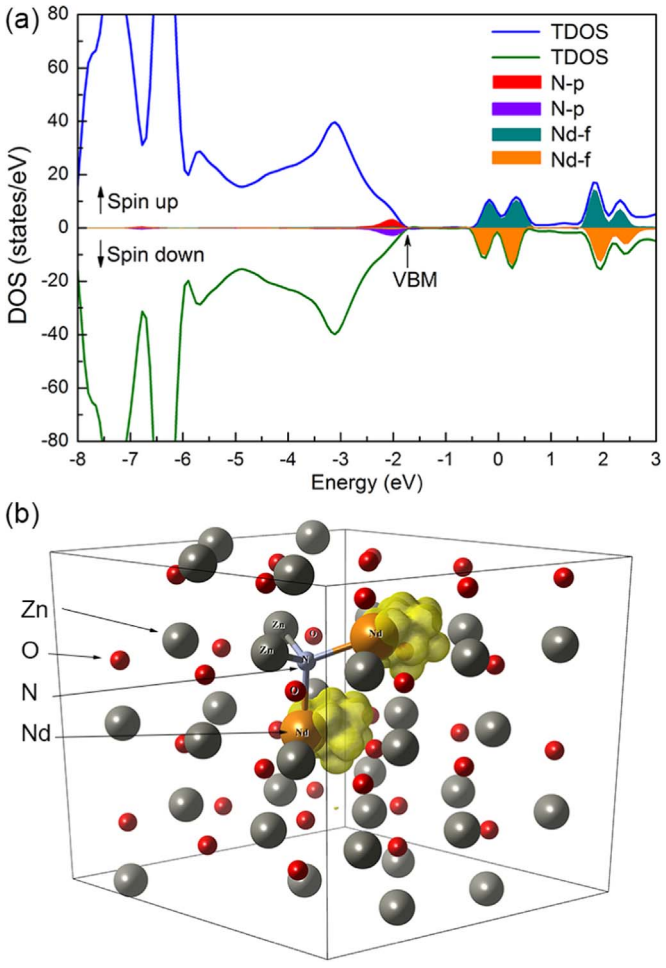

Fig. 6. (a) Calculated total and partial DOS and (b) spin density distributions of the 72-atom ZnO supercell with $2Nd_{Zn}$-N_O complex. The Fermi level is set at zero.

supporting the observed room temperature magnetism. In order to further determine whether the formation of the $2Nd_{Zn}$-N_O complex is stable in ZnO, we calculated the binding energy of the complex: $E_b=E_{tot}(2Nd_{Zn}$-$N_O)+E_{tot}(ZnO)-E_{tot}(2Nd_{Zn})-E_{tot}(N_O)$, where E_{tot} is the total energy of the system calculated with the same supercell. The calculated binding energy E_b for the $2Nd_{Zn}$-N_O complex is −1.7 eV, indicating that the complex is stable with respect to the isolated Nd and N dopants in ZnO.

To well understand the origin of ferromagnetism, the total and partial spin-resolved DOS of the ZnO system with $2Nd_{Zn}$-N_O complex were calculated, as shown in Fig. 6(a). There exists a significant spin splitting in the conduction band, which is contributed by the Nd-f states. We obtained a magnetic moment of 3.2 μB for each Nd atom. Fig. 6(b) shows the spatial distributions of spin density for the ZnO supercell with $2Nd_{Zn}$-N_O complex. Most of the spin densities were localized in the vicinity of Nd dopants, which was consistent with results from the DOS calculations.

4. Conclusions

In summary, we carried out a comparative study on magnetism of undoped, Nd-doped N-doped and (Nd, N)-codoped ZnO by combining experiments with first-principles calculations. Our results demonstrated unambiguously a ferromagnetism enhancement in (Nd, N)-codoped ZnO, suggesting that donor-acceptor complex plays a key role for establishing ferromagnetic order in ZnO.

Acknowledgements

This work is supported by the National Natural Science Foundation of China under Grant Nos. 10874178, 11074093, 61205038 and 11274135, Specialized Research Fund for the Doctoral Program of Higher Education under Grant No. 20130061130011, Ph.D. Programs Foundation of Ministry of Education of China under Grant No. 20120061120011, Natural Science Foundation of Jilin Province under grant No. 201115013. The Science and Technology Development Project of Jilin Province under grant No. 20170101142JC. This work was also supported by High Performance Computing Center of Jilin University, China.

References

[1] I. Žutić, J. Fabian, S. Das Sarma, Spintronics: fundamentals and applications, Rev. Mod. Phys. 76 (2) (2004) 323–410.
[2] S.A. Wolf, D.D. Awschalom, R.A. Buhrman, J.M. Daughton, S. von Molnár, M.L. Roukes, A.Y. Chtchelkanova, D.M. Treger, Spintronics: a spin-based electronics vision for the future, Science 294 (5546) (2001) 1488.
[3] H. Ohno, Making nonmagnetic semiconductors ferromagnetic, Science 281 (5379) (1998) 951–956.
[4] H. Ohno, Toward functional spintronics, Science 291 (5505) (2001) 840.
[5] J. Blinowski, P. Kacman, J.A. Majewski, Ferromagnetic superexchange in Cr-based diluted magnetic semiconductors, Phys. Rev. B 53 (15) (1996) 9524–9527.
[6] T. Dietl, A ten-year perspective on dilute magnetic semiconductors and oxides, Nat. Mater. 9 (12) (2010) 965–974.
[7] A.G. El Hachimi, H. Zaari, M. Boujnah, A. Benyoussef, M. El Yadari, A. El Kenz, Ferromagnetism induced by oxygen related defects in CeO_2 from first principles study, Comput. Mater. Sci. 85 (2014) 134–137.
[8] S.J. Pearton, D.P. Norton, M.P. Ivill, A.F. Hebard, J.M. Zavada, W.M. Chen, I.A. Buyanova, ZnO doped with transition metal ions, IEEE Trans. Electron Devices 54 (5) (2007) 1040–1048.
[9] F. Pan, C. Song, X.J. Liu, Y.C. Yang, F. Zeng, Ferromagnetism and possible application in spintronics of transition-metal-doped ZnO films, Mater. Sci. Eng. R: Rep. 62 (1) (2008) 1–35.
[10] M.H.F. Sluiter, Y. Kawazoe, P. Sharma, A. Inoue, A.R. Raju, C. Rout, U.V. Waghmare, First principles based design and experimental evidence for a ZnO-based ferromagnet at room temperature, Phys. Rev. Lett. 94 (18) (2005) 187204.
[11] J. Anderson, G.Vd.W. Chris, Fundamentals of zinc oxide as a semiconductor, Rep. Prog. Phys. 72 (12) (2009) 126501.
[12] Q. Li, T.T. Shen, Z.K. Dai, Y.L. Cao, S.S. Yan, S.S. Kang, Y.Y. Dai, Y.X. Chen, G.L. Liu, L.M. Mei, Spin polarization of $Zn_{1-x}Co_xO$ probed by magnetoresistance, Appl. Phys. Lett. 101 (17) (2012) 172405.
[13] M.D. McCluskey, S.J. Jokela, Defects in ZnO, J. Appl. Phys. 106 (7) (2009) 071101.
[14] W. Prellier, A. Fouchet, B. Mercey, Oxide-diluted magnetic semiconductors: a review of the experimental status, J. Phys.: Condens. Matter 15 (37) (2003) R1583.
[15] S.B. Ogale, Dilute doping, defects, and ferromagnetism in metal oxide systems, Adv. Mater. 22 (29) (2010) 3125–3155.
[16] Y. Li, R. Deng, B. Yao, G. Xing, D. Wang, T. Wu, Tuning ferromagnetism in $Mg_xZn_{1-x}O$ thin films by band gap and defect engineering, Appl. Phys. Lett. 97 (10) (2010) 102506.
[17] T. Dietl, H. Ohno, F. Matsukura, J. Cibert, D. Ferrand, Zener model description of ferromagnetism in zinc-blende magnetic semiconductors, Science 287 (5455) (2000) 1019.
[18] P.V. Radovanovic, D.R. Gamelin, High-temperature ferromagnetism in Ni^{2+}-doped ZnO aggregates prepared from colloidal diluted magnetic semiconductor quantum dots, Phys. Rev. Lett. 91 (15) (2003) 157202.
[19] Y.-f. Tian, Y.-f. Li, T. Wu, Tuning magnetoresistance and exchange coupling in ZnO by doping transition metals, Appl. Phys. Lett. 99 (22) (2011) 222503.
[20] Y. Tian, Y. Li, M. He, I.A. Putra, H. Peng, B. Yao, S.A. Cheong, T. Wu, Bound magnetic polarons and p-d exchange interaction in ferromagnetic insulating Cu-doped ZnO, Appl. Phys. Lett. 98 (16) (2011) 162503.
[21] S.Z. Wu, H.L. Yang, X.G. Xu, J. Miao, Y. Jiang, Ferromagnetism studies of Cu-doped and (Cu, Al) co-doped ZnO thin films, J. Phys: Conf. Ser. 263 (2011) 012022.
[22] T. Dietl, Origin of ferromagnetic response in diluted magnetic semiconductors and oxides, J. Phys.: Condens. Matter 19 (16) (2007) 165204.
[23] S. Pearton, Recent progress in processing and properties of ZnO, Prog. Mater. Sci. 50 (3) (2005) 293–340.
[24] M.A. Garcia, E. Fernandez Pinel, J. de la Venta, A. Quesada, V. Bouzas, J.F. Fernández, J.J. Romero, M.S. Martín González, J.L. Costa-Krämer, Sources of experimental errors in the observation of nanoscale magnetism, J. Appl. Phys. 105 (1) (2009) 013925.
[25] S. Dhar, O. Brandt, M. Ramsteiner, V.F. Sapega, K.H. Ploog, Colossal magnetic moment of Gd in GaN, Phys. Rev. Lett. 94 (3) (2005) 037205.
[26] L. Liu, P.Y. Yu, Z. Ma, S.S. Mao, Ferromagnetism in GaN:Gd: a density functional theory study, Phys. Rev. Lett. 100 (12) (2008) 127203.
[27] M. Ungureanu, H. Schmidt, Q. Xu, H. von Wenckstern, D. Spemann, H. Hochmuth, M. Lorenz, M. Grundmann, Electrical and magnetic properties of RE-doped ZnO thin films (RE=Gd, Nd), Superlattices Microstruct. 42 (1–6) (2007) 231–235.
[28] Y. Li, R. Deng, W. Lin, Y. Tian, H. Peng, J. Yi, B. Yao, T. Wu, Electrostatic tuning of Kondo effect in a rare-earth-doped wide-band-gap oxide, Phys. Rev. B 87 (15) (2013) 155151.
[29] G. Vijayaprasath, R. Murugan, T. Mahalingam, Y. Hayakawa, G. Ravi, Enhancement of ferromagnetic property in rare earth neodymium doped ZnO nanoparticles, Ceram. Int. 41 (9) (2015) 10607–10615.
[30] H. Shi, P. Zhang, S.-S. Li, J.-B. Xia, Magnetic coupling properties of rare-earth metals (Gd, Nd) doped ZnO: first-principles calculations, J. Appl. Phys. 106 (2) (2009) 023910.
[31] K.R. Kittilstved, W.K. Liu, D.R. Gamelin, Electronic structure origins of polarity-dependent high-TC ferromagnetism in oxide-diluted magnetic semiconductors, Nat. Mater. 5 (4) (2006) 291–297.
[32] D.D. Wang, G.Z. Xing, F. Yan, Y.S. Yan, S. Li, Ferromagnetic (Mn, N)-codoped ZnO nanopillars array: experimental and computational insights, Appl. Phys. Lett. 104 (2) (2014) 022412.
[33] Y. Li, R. Deng, Y. Tian, B. Yao, T. Wu, Role of donor-acceptor complexes and impurity band in stabilizing ferromagnetic order in Cu-doped SnO_2 thin films, Appl. Phys. Lett. 100 (17) (2012) 172402.
[34] G. Kresse, J. Furthmüller, Efficient iterative schemes for ab initio total-energy calculations using a plane-wave basis set, Phys. Rev. B 54 (16) (1996) 11169.
[35] G. Kresse, J. Furthmüller, Efficiency of ab-initio total energy calculations for metals and semiconductors using a plane-wave basis set, Comput. Mater. Sci. 6 (1) (1996) 15–50.
[36] P.E. Blöchl, Projector augmented-wave method, Phys. Rev. B 50 (24) (1994) 17953.
[37] J.P. Perdew, K. Burke, M. Ernzerhof, Generalized gradient approximation made simple, Phys. Rev. Lett. 77 (18) (1996) 3865.
[38] R.D. Shannon, Revised effective ionic radii and systematic studies of interatomie distances in halides and chaleogenides, Acta Cryst. A32 (1976) 751–767.
[39] S.R. Naik, T. Shripathi, A.V. Salker, Preparation, characterization and photoluminescent studies of Cr and Nd co-doped Ce:YAG compounds, J. Lumin. 161 (2015) 335–342.
[40] X.H. Li, H.Y. Xu, X.T. Zhang, Y.C. Liu, J.W. Sun, Y.M. Lu, Local chemical states and thermal stabilities of nitrogen dopants in ZnO film studied by temperature-dependent x-ray photoelectron spectroscopy, Appl. Phys. Lett. 95 (19) (2009) 191903.
[41] H.Y. Wei, Y.S. Wu, L.L. Wu, C.X. Hu, Preparation and photoluminescence of surface N-doped ZnO nanocrystal, Mater. Lett. 59 (2–3) (2005) 271–275.
[42] J. Tauc, Amorphous and Liquid Semiconductors, Plenum Press, New York, 1974.
[43] K. Ellmer, Resistivity of polycrystalline zinc oxide films: current status and physical limit, J. Phys. D: Appl. Phys. 34 (21) (2001) 3097.
[44] V. Kumar, R.G. Singh, L.P. Purohit, R.M. Mehra, Structural, transport and optical properties of boron-doped zinc oxide nanocrystalline, J. Mater. Sci. Technol. 27 (6) (2011) 481–488.
[45] Y. Gai, J. Li, S.-S. Li, J.-B. Xia, S.-H. Wei, Design of narrow-gap TiO_2: a passivated codoping approach for enhanced photoelectrochemical activity, Phys. Rev. Lett. 102 (3) (2009) 036402.
[46] D. Theyvaraju, S. Muthukumaran, Preparation, structural, photoluminescence and magnetic studies of Cu doped ZnO nanoparticles co-doped with Ni by sol–gel method, Physica E 74 (2015) 93–100.
[47] D. Gao, Z. Zhang, J. Fu, Y. Xu, J. Qi, D. Xue, Room temperature ferromagnetism of pure ZnO nanoparticles, J. Appl. Phys. 105 (11) (2009) 113928.
[48] S. Banerjee, M. Mandal, N. Gayathri, M. Sardar, Enhancement of ferromagnetism

upon thermal annealing in pure ZnO, Appl. Phys. Lett. 91 (18) (2007) 182501.
[49] Ö. Altıntaş Yıldırım, C. Durucan, Room temperature synthesis of Cu incorporated ZnO nanoparticles with room temperature ferromagnetic activity: structural, optical and magnetic characterization, Ceram. Int. 42 (2) (2016) 3229–3238.
[50] B. Cao, W. Cai, H. Zeng, Temperature-dependent shifts of three emission bands for ZnO nanoneedle arrays, Appl. Phys. Lett. 88 (16) (2006) 161101.
[51] O. Altintas Yildirim, Y. Liu, A.K. Petford-Long, Synthesis of uniformly distributed single- and double-sided zinc oxide (ZnO) nanocombs, J. Cryst. Growth 430 (2015) 34–40.
[52] C. Liu, H. He, L. Sun, Q. Yang, Z. Ye, L. Chen, Correlation between the 3.31-eV emission and the doping level in indium-doped ZnO nanostructures, Solid State Commun. 150 (47–48) (2010) 2303–2305.
[53] M. Schirra, R. Schneider, A. Reiser, G.M. Prinz, M. Feneberg, J. Biskupek, U. Kaiser, C.E. Krill, K. Thonke, R. Sauer, Stacking fault related 3.31-eV luminescence at 130 meV acceptors in zinc oxide, Phys. Rev. B 77 (12) (2008) 125215.
[54] J.W. Sun, Y.M. Lu, Y.C. Liu, D.Z. Shen, Z.Z. Zhang, B. Yao, B.H. Li, J.Y. Zhang, D.X. Zhao, X.W. Fan, Nitrogen-related recombination mechanisms in p-type ZnO films grown by plasma-assisted molecular beam epitaxy, J. Appl. Phys. 102 (4) (2007) 043522.
[55] Q. Wang, Q. Sun, G. Chen, Y. Kawazoe, P. Jena, Vacancy-induced magnetism in ZnO thin films and nanowires, Phys. Rev. B 77 (20) (2008) 205411.
[56] L. Shen, R.Q. Wu, H. Pan, G.W. Peng, M. Yang, Z.D. Sha, Y.P. Feng, Mechanism of ferromagnetism in nitrogen-doped ZnO: first-principle calculations, Phys. Rev. B 78 (7) (2008) 073306.